Room temperature ferromagnetism in Sb doped ZnO

Luo, C.-Q.; Zhu, S.-C.; Xu, C.; Zhou, S.; Lame, C.-H.; Ling, F. C.-C.;

Originally published:

March 2021

Journal of Magnetism and Magnetic Materials 529(2021), 167908

DOI: https://doi.org/10.1016/j.jmmm.2021.167908

Perma-Link to Publication Repository of HZDR:

https://www.hzdr.de/publications/Publ-32726

Room Temperature Ferromagnetism in Sb doped ZnO

Cai-Qin Luo[1,2*], Si-Cong Zhu[3], Chi Xu[4], Shengqiang Zhou[4], Chi-Hang Lam[5], Francis Chi-Chung Ling[2*]

[1]*Henan Key Laboratory of Photovoltaic Materials, Henan University, Kaifeng, China*
[2]*Department of Physics, The University of Hong Kong, Pokfulam Road, Hong Kong, China*
[3]*College of Science and Key Laboratory for Ferrous Metallurgy and Resources Utilization of Ministry of Education, Wuhan University of Science and Technology, Wuhan, China*
[4]*Institute of Ion Beam Physics and Materials Research, Helmholtz-Zentrum Dresden-Rossendorf, Bautzner Landstr. 400, 01328 Dresden, Germany*
[5]*Department of Applied Physics, Hong Kong Polytechnic University, Hung Hom, Hong Kong, China*

* Corresponding author: ccling@hku.hk, luocq17@foxmail.com

Abstract

Using first-principle calculations, the magnetic properties of the monovacancies and the Sb-related defects including V_{Zn}, V_O, Sb_{Zn}, Sb_O, Sb_{Zn}-V_{Zn} and Sb_{Zn}-$2V_{Zn}$ are studied. It is found that the isolated V_{Zn} with the charge state of 0 and -1 can contribute to ferromagnetism in ZnO material. The substitution of Sb on O sites (Sb_O^0) also results in magnetic property. Moreover, the Sb_{Zn}-$2V_{Zn}$ complex is another defect having non-zero magnetic moment and energetically favours for the ferromagnetic state. The resultant density of states (DOS) and spin density distribution clearly show that the ferromagnetic interaction is majorly due to the O-p Zn-d and Sb-p states. To check this calculation, Sb-doped ZnO samples were grown by pulsed laser deposition with different Sb composition under $P(O_2)$=1.3 Pa. SQUID study showed that all of these samples are ferromagnetic at room temperature. The variation of the saturation magnetization against the Sb composition is discussed.

Keywords

Sb-doped ZnO, defects, ferromagnetism, SQUID

Introduction

Extensive effort has been devoted to study dilute magnetic semiconductors (DMS) [1-4]. Many theoretical studies revealed the possibility of room temperature (RT) ferromagnetism (FM) introduced by dilute doping of magnetic ions in semiconductors, for example $Cd_{1-x}Mn_xSe$[5], $Zn_{1-x}Fe_xSe$[6], $Zn_{1-x}Mn_xO$[7], $Zn_{1-x}Co_xO$[8], etc. ZnO is a multi-functional material among these DMS [9]. There are many reports of RT FM observed in ZnO doped with a variety of transition metals like Co [10-15], Mn [10, 11, 16, 17], Fe [18] and Cu [19-21]. It was suggested that defects played crucial role in the intrinsic carrier mediated FM coupling [1, 17, 20, 21] and the presence of hole carrier could enhance the FM [22, 23]. It is not doubt that native defects, especially the dominant V_{Zn} and V_O, cannot be ruled out from the origin of RT FM. It is found that there is a correlation between the increase of V_O and the enhancement of ferromagnetism in Co doped ZnO [24]. The observed RT FM in Cu doped ZnO can be well interpreted by an indirect exchange model due to the presence of V_O and Cu impurities [25]. On the other hand, V_{Zn}, as one of the acceptors in ZnO with high concentration, can also be used to enhance ferromagnetism through increasing its concentration on purpose. Recently, strong FM was observed in undoped 2D ZnO by increasing V_{Zn} concentration to ~10^{22} cm^{-3} through H-passivated (forming V_{Zn}-H)[26], saturated magnetization (Ms) with value of 50.9 emu/g (around 285.4 emu/cm^3) is one to five orders of magnitude higher than the other published results. The robust Ms is also comparable with conventional ferromagnetic materials. Their findings indicated that the increase of V_{Zn} related defects in ZnO material with massive grain boundaries is likely to significantly increase RT FM. The origin of RT FM in undoped ZnO was focused in our previous work[27, 28]. The experimental observed RT FM can be attributed to the V_{Zn} related defects residing on the grain surface [28], and the follow-on computational study indicated the unit cells of ZnO containing the V_{Zn}, Oi(oct) and $2V_{Zn}$-V_O in the configuration

of a-b plane and c axis energetically favors for FM state. The isolated V_O prefers non-polarized state, thus is not the root cause for RT FM in undoped ZnO [27]. However, there were also disagreements that the observed RT FM was originated from extrinsic origins like magnetic nanometer-sized transition metal clusters [29], magnetic oxide and secondary phase [30], grain boundary [31, 32], and residual spin on non-magnetic oxide nanocluster [33, 34].

Majority of the DMS study on ZnO was concentrated on transition metal doped ZnO and few was devoted to the study on doping ZnO with non-transition metals like C [35] and Li [36]. There were experimental studies reporting Sb-doped ZnO to have p-type conductivity [37, 38]. But there were also literature observing n^+-conductivity in Sb-doped ZnO[39, 40]. Theoretical study [41] showed that Sb occupying Zn-site Sb_{Zn} is donor and Sb occupying O-site Sb_O is deep acceptor and Sb_O has a higher formation energy than Sb_{Zn}. Sb_{Zn}-$2V_{Zn}$ is a shallow acceptor having a low formation energy [41] and has been associated with the experimentally observed p-type conductivity or the defect compensating the electron carriers [39, 42]. Interestingly, there is also other explanation for the observation of p-type conductivity in Sb doped ZnO. Andrew et al [43] reported that Sb doping in ZnO nanowire can lead to stable p-type conduction due to O-doping stabilized by Sb decorated head-to-head basal planed inversion domain boundaries. The presence of Sb switches the surface polarity and also incorporates an extra O basal plane positioned at the polarity-switch node. Besides, it is also found that Sb doping may have influence on the formation of V_{Zn} on ZnO surface [44], the beneath Sb was predicted to enhance the driving force to align the vacancy pattern on surface/ or boundaries. It is reasonable to speculate the introduction of Sb in ZnO may affect the exotic physical properties like RT FM, which is the objective of the present study.

The concentration change of intrinsic defect and the presence of the acceptor defects in Sb-doped ZnO material could enhance magnetic property, and few efforts were devoted to study the influence of Sb dopant on the ferromagnetism in ZnO. In the present study, first

principle calculation was carried out to study the magnetic properties of the Sb-related defects in ZnO, namely Sb_{Zn}, Sb_O, Sb_{Zn}-V_{Zn} and Sb_{Zn}-$2V_{Zn}$. By using the DFT method, we examine the relaxed atomic geometry, the formation energy and the induced magnetic moment of these defects. Sb_O and Sb_{Zn}-$2V_{Zn}$ in the zero charge states have non-zero magnetic moment and their ferromagnetic states are more energetic favourable than their anti-ferromagnetic states. Sb-doped ZnO samples were grown by pulsed laser deposition with their magnetic properties characterized. The experimental findings are discussed with the theoretical results.

Methods for theoretical calculations

The total energy and electronic structure calculations were performed based on the density functional theory (DFT) as implemented in the Vienna ab *initio* Simulation Package. A spin-polarized generalized gradient approximation (SGGA) with Perdew-Burke-Ernzerhof (PBE) was adopted. A plane-wave energy cutoff of 400 eV is used for the plane-wave expansion of the electronic wave function, with a 3×3×3 Monkhorst-pack mesh grid as k point sampling throughout the calculations. The test calculations with denser k grid and higher cutoff energy give effective identical results. A 3×3×2 supercell with 72 atoms is used to build defective bulk ZnO. All atoms in the supercell were allowed to move during the structural optimization until relaxed to their equilibrium positions such that forces are converged to less than 0.01 eV/A and the energy converged to less than10^{-5} eV/atom. The calculated bandgap of undoped ZnO is around 1.3 eV, which is smaller than that of the experimental value ~3.3 eV. The band-gap discrepancy is commonly seen due to the failures of approximate exchange-correction functional, and no U parameter was used through the calculations.

Experimental Methods

The undoped ZnO film and Sb-doped ZnO films with different Sb composition were grown on c-plane sapphire substrates with oxygen partial pressure (P(O2)) of 1.3 Pa or 0 Pa using pulsed laser deposition (PLD). The substrate temperature was kept at 350 ℃ during growth. The details of the growth can be found in reference [39]. The magnetic properties of the samples were characterized using the Quantum Design Superconducting Quantum Interference Device-Vibrating sample Magnetometer (SQUID). These samples have been characterized using a comprehensive approach, namely Hall effect measurement, X-ray diffraction (XRD), photoluminescence (PL), X-ray photoelectron spectroscopy (XPS) and positron annihilation spectroscopy (PAS). The results were presented in reference[39].

Results of theoretical study

All the atoms are fully relaxed to the equilibrium position during structural optimization. It is worthy to discuss the relaxation effects for future reference. For the intrinsic point defects, V_O with +2 charge state causes the most significant displacement, the first neighboring Zn atoms move outward by 24%. The nearest Zn atoms are less displaced for the neutral and +1 state of V_O, with 12.3% and 0.3% inward shift compared with the ideal Zn-O bond length. Unlike V_O, the relaxation of V_{Zn} has no dependence on its charge state, the displacement is around 10.6%. The occupation of Sb on O sites (Sb_O) has a tremendous effect on the nearest Zn and O atoms, which displace outward by 28% and 21% respectively. For the Sb_{Zn} with +2 and +3 charge state, the displacement for the near Zn and O atoms can be neglected. For Sb_{Zn}-V_{Zn}, the Sb atom tends to move forward to the direction of V_{Zn}. It is

interesting to note that Sb on Zn site with two near V_{Zn} (Sb_{Zn}-$2V_{Zn}$) tends to form a five-fold structure. Sb atom shifts downward and the beneath O atom moves upward to shorten the bond-length, which is still 1.6% longer than the ideal bond length of Zn-O. The relaxation results have no significant difference for Sb_{Zn}-$2V_{Zn}$ with neutral, -1 and -2 charge states.

Table I The Calculated cell parameters a, c, α and γ for pure ZnO and Sb doped ZnO with different type of defects, c/a and cell volume are also included.

sample	Lattice parameter					Volume (Å^3)
	a (Å)	c (Å)	α (°)	γ (°)	c/a	
perfect ZnO	3.257	5.240	90	120	1.609	48.138
V_O	3.244	5.220	90	120	1.609	47.572
V_{Zn}	3.251	5.238	90	120	1.611	47.942
Sb_O	3.276	5.308	90	120	1.620	49.333
Sb_{Zn}	3.267	5.292	90	120	1.620	48.914
Sb_{Zn}-V_{Zn}	3.267	5.242	90	120	1.605	48.452
Sb_{Zn}-$2V_{Zn}$	3.268	5.221	90	120	1.598	48.288

The lattice parameters were calculated for the 72 atom ZnO supercell for the perfect ZnO lattice. The a and c parameters are found to be 3.257 Å and 5.240 Å respectively, which are ~0.7 % larger than the experimental values [45]. The effects of introducing a single defect of V_O, V_{Zn}, Sb_O, Sb_{Zn}, Sb_{Zn}-V_{Zn} and Sb_{Zn}-$2V_{Zn}$ into the 72 atom ZnO supercell were also studied. The defect concentration introduced on purpose is around 1.1 $\times 10^{21}$ cm^{-3}, which is comparable to the value observed from experimental study [39]. The change of ZnO general parameters obtained from the theoretical restults can be used to indicate the type of defects. The resultant a and c parameters of the ZnO supercell with the addition of one such defect are tabulated in Table I. The presence of V_O or V_{Zn} with concentration of ~10^{21} cm^{-3} have the effects of reducing the a-parameters to 3.244 Å and 3.251 Å and the c-parameters to 5.220 Å and 5.238 Å, respectively. The introductions of the Sb_O and the Sb_{Zn} into the supercell increase the a-parameters to 3.276 Å and 3.267 Å and the c-parameters to 5.308 Å and 5.292

Å respectively. For the V_{Zn}-related defect complexes Sb_{Zn}-V_{Zn} and Sb_{Zn}-$2V_{Zn}$, their presence in the supercell increase the a-parameter to 3.267 Å and 3.268 Å respectively, while their c-parameters change to 5.242 Å and 5.221 Å respectively.

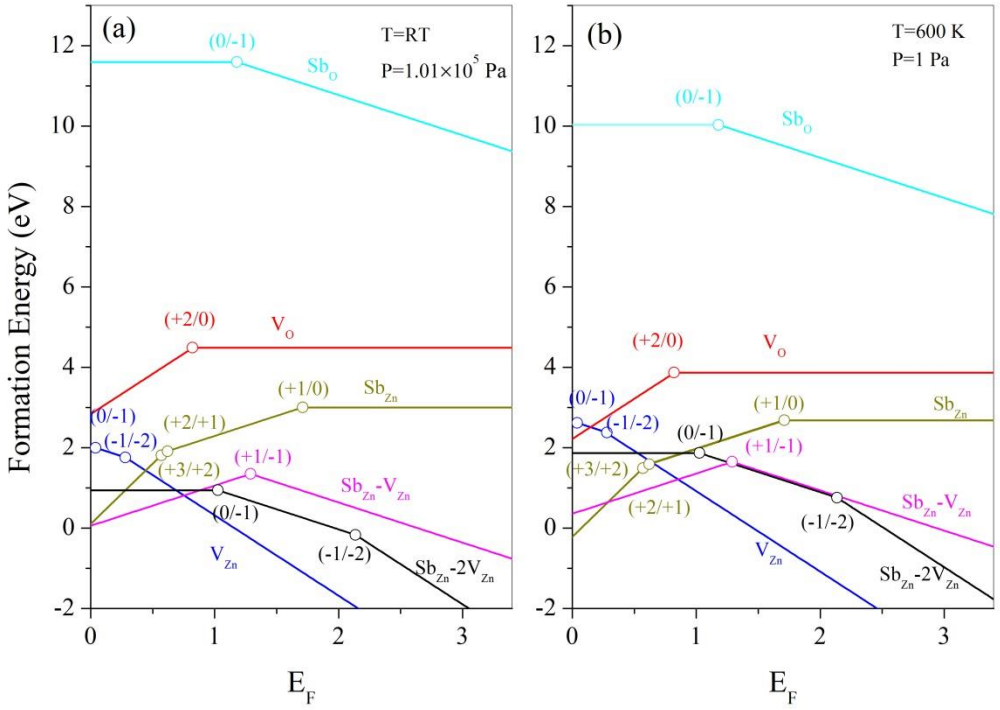

Figure 1 *Formation energies of defects in Sb doped ZnO material as a function of Fermi-level, (a) standard condition, (b) condition of the interest. The Zero-point of Fermi-level corresponds to the top of valence-band. The slope represents the charge state, and only the lowest-energy state is shown. The square points in the curves indicate the transition levels in the band gap.*

The concentration of the defect n is related to its formation energy under the equilibrium situation [46] via:

$$n = N_{sites}\exp\left(-\frac{E^f}{k_B T}\right) \qquad (1)$$

where E^f is the formation energy, k_B is the Boltzmann constant and T is the temperature. The energy of defect formation in ZnO as function of defect species X, charge state q, and temperature T and oxygen partial pressure P is giver as[47, 48]:

$$E^f(X^q) = E_{tot}(X^q) - E_{tot}(ZnO, perfect) - \sum n_i \mu_i(T,P) + q(E_V + E_F + \Delta V) \quad (2)$$

where $E^f(X^q)$ is the formation energy of defect X in ZnO cell, q is the charge state of defect X, $E_{tot}(X^q)$is the calculated total energy of a supercell having defect X in charge state q, E_{tot}(ZnO,perfect) is the total energy of a perfect supercell without any defect. n_i is the number of atoms (type i) that have been removed (n_i>0) or added (n_i<0) when the defect is formed. μ_i (T,P)is the corresponding chemical potentials of the elemental species as function of temperature and oxygen partial pressure. E_V is valence-band maximum of ZnO bulk, which is defined as $E_V = E_{tot}^{q=0}(ZnO, perfect) - E_{tot}^{q=1}(ZnO, perfect)$. E_F is referenced to the valence-band maximum. ΔV is added as a correction term to align the reference potential in the defective supercell with that in the perfect bulk. In present study, to line up the Fermi-level between different calculations, we align the electrostatic potentials by inspecting the potential in the supercell far from the defect and aligning it with electrostatic potential in defect-free ZnO supercell [49, 50]. Fermi level E_F is treated as a variable. The chemical potentials of the elemental species depend on the experimental growth conditions, and are treated as variables in equation (2). It is physically meaningful to place some bounds on the chemical potentials in thermodynamic equilibrium. Finnis et al [51, 52] developed an approach to obtain the oxygen chemical potential (μ_O(P,T)) in terms of temperature T and oxygen partial pressure P:

$$\mu_O(P,T) = \mu_O(T^0, P^0) + \Delta\mu_O^0(T) + \frac{1}{2}k_B T log\left(\frac{P_{O_2}}{P^0}\right) \quad (3)$$

Here μ_O (T^0,P^0) is the reference point of oxygen chemical potential at standard temperature (room temperature) and pressure (1 atm). In present study, we take the value

$\mu_O(T^0, P^0)=\frac{1}{2}\mu_{O2}(T^0,P^0)$=-4.19 eV from the previously calculation [53] based on a strategy to invoke a thermodynamic cycle corresponding to formation of some oxide. $\Delta\mu_O^0$ (T) = -1/2 $[(S_{O2}^0-C_P^0)(T-T^0)+C_P^0 Tln(T/T^0)]$ is the difference in oxygen chemical potential between standard temperature obtained from thermodynamic data to temperature of interest. S_{O2}^0 is the entropy of oxygen gas obtained from to thermodynamic data, and C_P^0 is $7k_B/2$. In our previous work, Sb doped ZnO films were grown at temperature of 600 K with oxygen partial pressure P＜10 Pa, which is also the condition of interest in present study. Given the circumstances, the calculated $\Delta\mu_O^0$ (T) is around -0.32 eV, and the last term of Equation (2) is roughly -0.30 eV with T=600K and P=1 Pa, there is no much difference (60 meV) as P increase to 10 Pa. The Zn and Sb chemical potential was derived from μ_{Zn}(T, P) = ΔH (ZnO)-μ_O(T, P), and μ_{Sb}(T, P)=1/2[ΔH (Sb_2O_3)-3μ_O(T, P)]. ΔH (ZnO) and ΔH (Sb_2O_3) are the obtain the enthalpies.

The growth condition plays critical role in the dopant and intrinsic defects concentration. Thus it is important to discuss the defects formation under certain circumstance. Figure 1 shows the formation energies for the defects (namely V_{Zn}, Sb_O, Sb_{Zn}, Sb_{Zn}-V_{Zn}, and Sb_{Zn}-2V_{Zn}) as a function of the Fermi-level. Different charge states of the defect refer to the different slopes of the straight lines, and the turning points correspond to the ionization states of the defect in the band gap. It is noticed that the as found ionization states in Figure 1 would be slightly different from the published result [42], which may be due to the different parameters and methodology used during the calculation. For the Sb point defects, Sb_{Zn} always has lower formation energy than Sb_O regardless of the oxygen abundance and the E_F position. This phenomenon is due to the sizing effect, the Sb^{3+} ionic radius (0.62 Å) is close to that of Zn^{2+} having values of 0.74 Å, while the ionic radius of Sb^{3-} is much larger than that of O^{2-}. Consequently, the Sb dopant is thus more likely to occupy the Zn-site of the ZnO lattice. For the condition with the standard room temperature ($T=T^0$) at the

standard pressure ($P=P^0$), V_{Zn}, Sb_{Zn}-V_{Zn} and Sb_{Zn}-$2V_{Zn}$ have relatively lower formation energies than the other defects as E_F is close to the conduction band minimum (CBM). Sb_{Zn} and Sb_{Zn}-V_{Zn} have low formation energies as E_F is close to the valence band minimum (VBM). For the case of the condition of our interest in present study, the ordering of defects with very low energies has little difference compared with the standard condition irrespective of the position of Fermi-level.

Table II. Total magnetic moments per unit cell (containing 72 atoms) with different kinds of defects. The energy difference ΔE between AFM and FM (E_{AFM}-E_{FM}) are calculated using a twice larger unit cell (144 atoms unit cell), the separation distance is around 9.8 Å. The non-polarized states are not included.

Defect type	Charge state	Moment(μ_B)	ΔE(meV)
V_{Zn}	0	1.82	38
	-1	0.99	31
Sb_O	0	1.04	19
Sb_{Zn}-V_{Zn}	0	0.96	-14
Sb_{Zn}-$2V_{Zn}$	0	0.64	22
Sb_{Zn}	2+	0.85	-39

Table II tabulates the total magnetic moments of the supercell containing the different defects having non-zero magnetic moments. The total energy difference between the ferromagnetism (FM) and anti-ferromagnetism (AFM) states (E_{AFM}-E_{FM}) were also calculated with the results tabulated in Table II. V_{Zn} with the charge states of 0 and -1 have magnetic moments of 1.82μ_B and 0.99μ_B respectively and their FM states are energetically favourable while compared with AFM states. This result is similar to those of the theoretical studies found in references [54]. It is noted that the energy difference ($\Delta E = E_{AFM} - E_{FM}$) for V_{Zn} is around 38 meV, which is large enough to lead to room-temperature ferromagnetism. Sb_O^0 also energetically favours FM ordering with a relatively small $\Delta E \sim 20$ meV and a non-zero magnetic moment of 1.04 μ_B. The shallow acceptor Sb_{Zn}-$2V_{Zn}$ in the neutral charge state

possesses a non-zero magnetic moment of $0.64\mu_B$ and energetically favours the FM state ($\Delta E \sim 20$ meV).

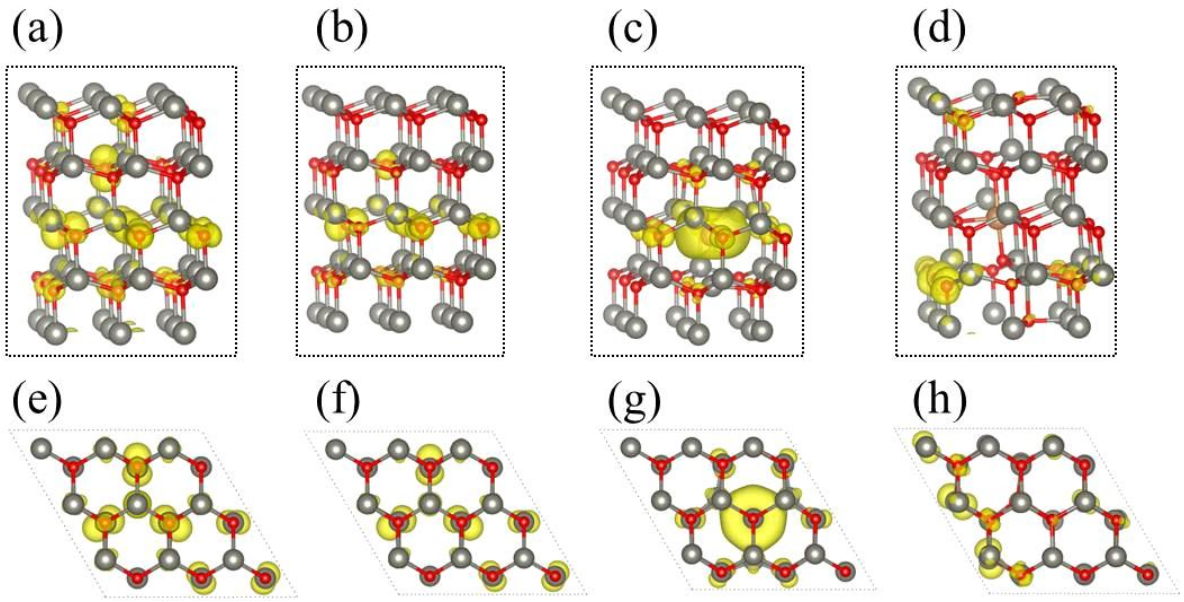

Figure 2 The side view of spin charge density distribution of ZnO with (a) V_{Zn}^0, (b) V_{Zn}^{1-}, and Sb doped ZnO with (c) Sb_O^0, (d) $(Sb_{Zn}\text{-}2V_{Zn})^0$; the corresponding top view of spin charge density distribution are shown in (e)-(h).

For the defects having non-zero magnetic moment and energetically favouring the ferromagnetic state, i.e. V_{Zn}^0, V_{Zn}^-, Sb_O^0 and $(Sb_{Zn}\text{-}2V_{Zn})^0$, their spin densities around the ions at 0 K in the corresponding supercell were calculated. Spin density is the difference between the spin-up and spin-down electrons. Figure 2 shows the three-dimensional iso-surface of the average spin charge density of 0.015 e/ Å. It is clearly seen in Figure 2(a), (e), (b), (f), (d) and (h) that for the supercell containing one V_{Zn} or one $Sb_{Zn}\text{-}2V_{Zn}$ the net magnetic moment is mainly contributed from the p electrons of the neighbouring O atom and second neighbouring O atom, and the magnetization diminishes as O atom is far from the V_{Zn}. Besides, Zn-d electrons also contribute to the magnetic moment. The contribution from Zn atoms is negligible as compared to that of O. For the case of Sb_O (figure 2(c) and (g)), the Sb substitution on O sites can also induce unpaired electron.

The total density of states (DOS) of ZnO with the defect V_{Zn}^{0}, V_{Zn}^{1-}, Sb_O^{0} and $(Sb_{Zn}\text{-}2V_{Zn})^{0}$ are shown in figure 3 (a), (b), (c) and (d) respectively. The band gaps of the supercells are found to be underestimated, which is commonly observed in GGA functional calculation. From figure 3 (a-e), the Fermi-level passes through the spin-down states, indicating the half metallic character of the ZnO systems with these defects. However, semiconductor behaviour of undoped ZnO and Sb-doped ZnO were observed experimentally. This is due to the underestimation of the exchange splitting of the GGA functional calculation. The asymmetric DOSs for the spin-up and spin-down electrons around the Fermi-level indicate the presence of the unpaired spins, which are consistent with the spin density distribution results as shown in figure 2. The partial DOS's of the atoms contributing to the FM of the supercell containing one V_{Zn}^{0}, V_{Zn}^{-}, Sb_O^{0} and $(Sb_{Zn}\text{-}2V_{Zn})^{0}$ are shown in the inserts of Figure 3(a-d) respectively. For the case of V_{Zn}^{0}, V_{Zn}^{-1} and $(Sb_{Zn}\text{-}2V_{Zn})^{0}$ shown in the inserts of Figure 3(a), (b) and (d) respectively, intense coupling of Zn-d and O-p states around the Fermi-level is observed. This indicates that the ferromagnetism induced by V_{Zn}^{0}, V_{Zn}^{-1} and $(Sb_{Zn}\text{-}2V_{Zn})^{0}$ are due to the p-d electron exchange between the Zn and O ions near the V_{Zn} defects. For the case of Sb_O shown in the inset of Figure 3(c) with the O-p, Zn-d and Sb-p states, the spin interaction is mainly due to the hybridization between the O-p and Sb-p states. The ferromagnetism induced by Sb_O is mediated through the p-p electron exchange interaction between O and Sb ions, Zn ions are also assignable for the ferromagnetism for the Sb_O case.

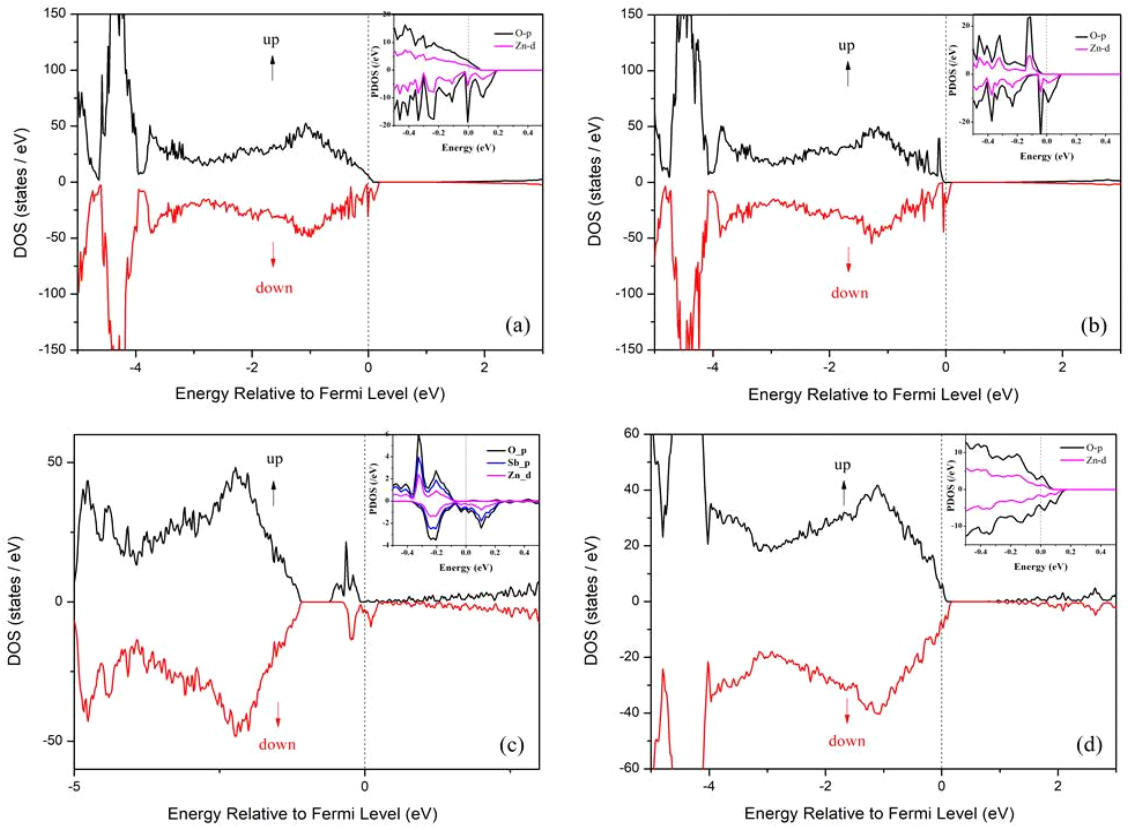

Figure 3 Total density of states of ZnO with (a) V_{Zn}^{0}, (b) V_{Zn}^{1-}, and Sb doped ZnO with (c) Sb_O^{0}, (d) $(Sb_{Zn}\text{-}2V_{Zn})^{0}$. The corresponding inset figure gives the partial DOS for the atoms that contribute to ferromagnetism.

Results of experimental study

A systematic magnetic study was carried out on Sb-doped ZnO samples, which were grown with P (O_2) =1.3 Pa or 0 Pa and with different Sb composition of 0 %, 0.5 %, 1 %, 2 % and 3 %. The M-H curves in Figure 4 (a) show that all the Sb-doped ZnO samples are ferromagnetic. The M-H curve of an undoped ZnO sample grown with P(O_2)=1.3 Pa is also included in Figure 4(a). The insert of Figure 4 (a) shows the saturation magnetization against the Sb composition whereas the samples are grown with P(O_2)=1.3 Pa. The undoped ZnO film has the saturation magnetization of 0.34 emu/cm^3. The saturation magnetization (Ms) is doubled to 0.64 emu/cm^3 upon the introduction of 0.5 % Sb. As the Sb composition increases

to 2 %, the saturation magnetization abruptly drops to 0.2 emu/cm^3. It then increases slightly to 0.3 emu/cm^3 as the Sb composition further increases to 3 %. The reference sample (2% Sb doped ZnO film prepared with P(O_2)=0 Pa) was grown to investigate the oxygen influence on RT FM. It is observed from figure 4(b) that the ferromagnetism can be enhanced (the value of Ms almost doubled) as the oxygen partial pressure decrease from 1.3 Pa to 0 Pa, which indicate that chemical potential of oxygen can change the defect structure in Sb doped ZnO film, which in turn adjust the magnetic property. RT ferromagnetism was also observed in other Sb doped ZnO material, it seems that polycrystalline sample obtained by sintered [55] or using aqueous reaction [56] have much weaker FM compared with epitaxial thin films grown using physical vapor deposition [57]. It is generally accepted that the ferromanetism of Sb doped ZnO material is assigned to V_{Zn} related defects. Doping Sb element into ZnO matrix could introduce more V_{Zn} and create a shallow acceptor defect Sb_{Zn}-$2V_{Zn}$. The 2p-electrons of the neighboring oxygen atoms would occupy virtual energy level and form into a spin polarized state [57]. The previous proposal to explain the origin of FM in Sb doped ZnO can be confirmed by the present theoretical calculation.

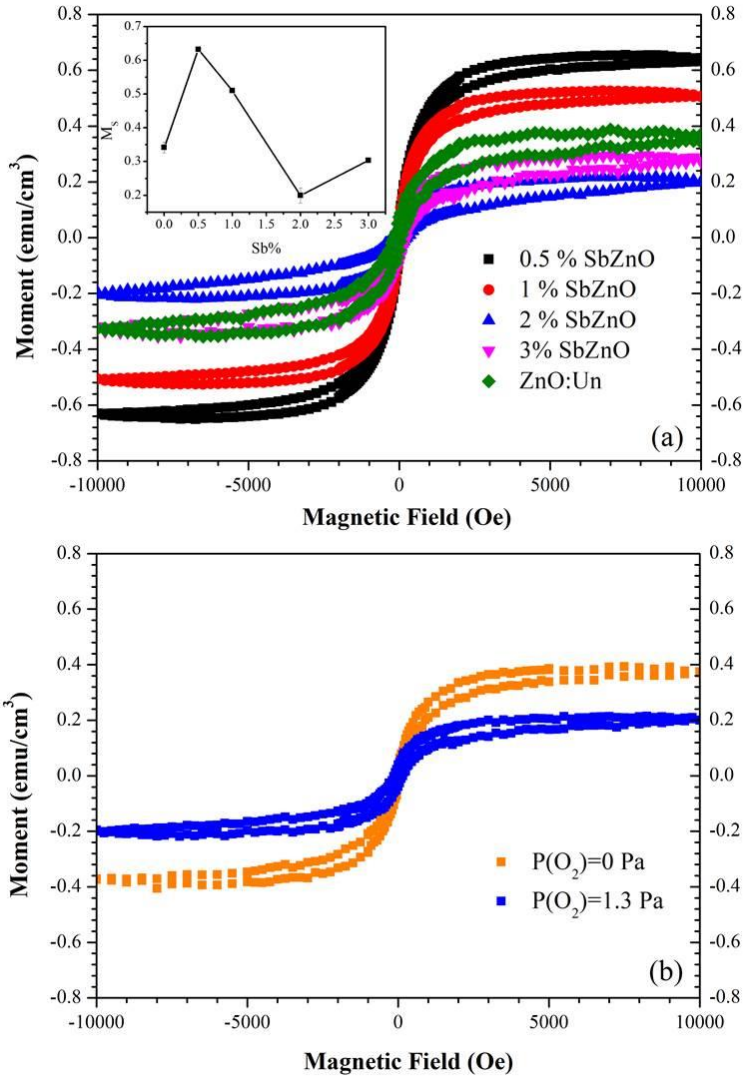

Figure 4 *Room temperature M-H loops of the Sb doped ZnO films: (a) the samples were grown under (a) P(O_2)=1.3 Pa with different Sb concentration, the inset figure shows magnetization as a function of Sb concentration; (b) 2% Sb doped ZnO samples grown with P(O2)=0 Pa and 1.3 Pa.*

Discussion and Conclusion

In reference [39], we have performed a comprehensive and systematic study on Sb-doped ZnO samples grown with the same PLD system and methodology as the present study using a multi-spectroscopic approach, including temperature dependent Hall measurement, PAS, PL, SIMS, XRD and XPS. For the samples with Sb composition≤ 2 %, the samples were n^+-type with electron concentration $>10^{20}$ cm^{-3}. It is also noticed that the electron concentration increases linearly with the Sb composition, and their values were very close.

According to the present calculation, the formation energy of Sb_{Zn} is significantly smaller than that of Sb_O thus implying the occupation of the Sb dopant at the Zn-site rather than the O-site. First principles calculation [42] showed that Sb_{Zn} is a donor and Sb_O is an acceptor. The shallow donor responsible for the n^+-conductivity was thus attributed to Sb_{Zn} or the Sb_{Zn} defect complex. As the Sb composition increases to 3 %, the conductivity of the sample abruptly changed from n^+ to n-type highly resistive. XRD study showed that the c-parameters of the samples with 1 % and 2 % of Sb were effectively the same as ~5.21 Å, but increasing the Sb composition to 3 % abruptly increased the c-parameter to 5.36 Å. The increase of the c-parameter could be due to the occupation of the Sb at the O-site rather than the Zn-site. The dramatic change of the conductivity from n^+ to highly resistive could be due to the formation of the Sb_O (or related defect complex) compensating acceptor and the drop of the Sb_{Zn} abundance. Liu e al [40] studied the MBE grown Sb-doped ZnO. A similar drop of electron concentration from $n^+ > 10^{20}$ cm^{-3} to $n \sim 10^{19}$ cm^{-3} was observed as the Sb concentration exceeded a threshold of $\sim 4\times10^{21}$ cm^{-3}, which was correlated with the abrupt increase of c-parameter revealed by XRD. The authors also attributed the shallow donor to Sb_{Zn} related defect, while the drop of the electron concentration was due to the Sb occupying the O-site rather than the Zn-site.

The present theoretical calculation shows that V_{Zn}, Sb_O and Sb_{Zn}-$2V_{Zn}$ could carry non-zero magnetization and have energetically stable FM state, whereas V_o, Sb_{Zn} and Sb_{Zn}-V_{Zn} do not have stable FM state with net magnetization. Using the similar computational method, we have studied the magnetic properties of V_{Zn}, V_O, $V_{Zn}V_O$, V_{Zn}-$2V_O$ and V_O-$2V_{Zn}$. It was found that some charge states of V_{Zn} V_{Zn}, $V_{Zn}V_O$ and V_O-$2V_{Zn}$ carry non-zero magnetic moment and their FM state are energetic stable. It is noticed that all of these ferromagnetic intrinsic defects contain V_{Zn}. Moreover, it is noticed that the V_O-rich defects V_O and V_{Zn}-$2V_O$ are not ferromagnetic. In the present experimental magnetic study, the

undoped ZnO sample is FM at room temperature. Its magnetic moment could be originated from the intrinsic defects V_{Zn} and the vacancy clusters $V_{Zn}V_O$ and V_O-$2V_{Zn}$.

With the low level doping of 0.5 % of Sb, the saturation magnetization is doubled as compared to the undoped sample, implying that the Sb has the effect of enhancing the magnetization. For the lowly Sb-doped ZnO samples, Sb occupies the Zn-site rather than the O-site, and Sb_{Zn} or its related defect complex is the shallow donor responsible for the n^+ conductivity [39]. According to the current theoretical calculation, Sb_{Zn} could carry non-zero magnetic moment but its AFM state is more energetic favourable than the FM state. The current study shows that Sb_O^0 carries non-zero magnetic moment and favours for the FM state. However, Sb_O^0 would not be the important contributor to the observed magnetization because Sb_{Zn} is the dominant site for Sb in this relatively low Sb composition sample. Thus, neither the Sb_{Zn} nor the Sb_O is the origin responsible for the enhanced saturation magnetization. Moreover from the current theoretical result, V_O nor Sb_{Zn}-V_{Zn} would contribute for the ferromagnetism. This implies that the V_{Zn} and Sb_{Zn}-$2V_{Zn}$ could be the candidates contributing to the ferromagnetism.

In our previous study, Luo et al [39] observed the self-compensation phenomenon in the n^+ Sb-doped ZnO samples, in which the acceptor (like V_{Zn}) concentration is enhanced to extraordinarily high (~10^{20} cm^{-3}) by the n^+ degenerate doping. Look et al [58] and Pak et al [59] observed the similar acceptor enhancement in degenerate Ga-doped ZnO. Using PAS, Look et al [58] further showed that the acceptor was associated with V_{Zn}. The self-compensation enhancement in V_{Zn} in n^+ degenerate ZnO sample is associated with the drop of the formation energy of acceptor while the Fermi level is close to the CBM (Figure 2 and Van de Walle [46]). The ZnO:Sb(0.5%) sample has saturation magnetization larger than the undoped ZnO sample. As it has just been pointed out that very high concentration of acceptor (~10^{20} cm^{-3}), which could be V_{Zn}, was identified in the n^+ Sb-doped [39]. The

increase of the saturated magnetization in the ZnO:Sb(0.5%) could be due to the abundant V_{Zn} formed because of self-compensation.

Coincidence Doppler broadening (CDB) spectroscopy is a kind of PAS which is selectively sensitive to V_{Zn} related defect. CDB spectroscopy can reveal the electronic momentum distribution in the vicinity of the Zn-vacancy in ZnO and thus able to identify the impurity decoration of the V_{Zn}. CDB study was performed on the as-grown Sb-doped ZnO samples fabricated with different Sb composition under $P(O_2)$=1.3 Pa which was the identical set of samples of the current study, as well as the control sample Sb. The electronic momentum distribution spectrum is presented as the ratio curve which is normalized against the defect-free ZnO single crystal. A peak at zero electronic momentum was found in the Sb control sample ratio curve, and this was the fingerprint feature of positron annihilating with Sb. This feature was not found in the undoped ZnO nor the lowly Sb-doped ZnO sample with Sb=1 %, but was identified in the Sb-doped ZnO sample with Sb=2 %. This was associated to the formation of the Sb-V_{Zn} defect complex, whereas positron at the V_{Zn} of this defect complex annihilated with the Sb valence electron and thus the corresponding ratio curve had the Sb feature. This implies isolated V_{Zn} exists in the undoped and the Sb(1 %) doped ZnO sample. As the Sb composition increases to 2 %, V_{Zn}-Sb type defect complex forms. Moreover, the formation of the V_{Zn}-Sb type defect complex is correlated with the introduction of the free to acceptor emission in the PL spectrum whereas the acceptor level agrees well with the theoretical value of the ionization energy of the Sb_{Zn}-$2V_{Zn}$ acceptor [42]. It can be concluded that Sb_{Zn}-$2V_{Zn}$ acceptor is formed as the Sb composition is raised to 2 %.

It would be worthy to discuss the origin of the drop of the magnetization as the Sb composition increases to 2 %. The observed RT FM in undoped ZnO could be originated from the V_{Zn} or the vacancy clusters $V_{Zn}V_O$ and V_O-$2V_{Zn}$ that carries non-zero magnetic moment and favours FM state. Doping the ZnO with 0.5 % Sb leads to the enhancement of

V_{Zn} concentration because of the self-compensation effect. As V_{Zn} contributes to magnetic moment, this results in the increase of saturation magnetization from the undoped sample of 0.34 emu/cm^{-3} to the value of 0.64 emu/cm^{3} for the 0.5 % Sb doped sample. As the Sb composition increases to 2 %, Sb_{Zn}-V_{Zn} defect complex exists in the sample rather than the $V_{Zn.}$, which leads to the drop of the saturation magnetization to 0.2 emu/cm^{3} because Sb_{Zn}-V_{Zn} does not favour the FM state and Sb_{Zn}-$2V_{Zn}$ has a smaller magnetic moment as compared to V_{Zn}. As Sb_{Zn} is not ferromagnetic, the formation of Sb_{Zn}-$2V_{Zn}$ is net effect of the removal of two V_{Zn} having high magnetic moment and forming one Sb_{Zn}-$2V_{Zn}$ having low magnetic moment.

Magnetic study was carried out on the as-grown 2% Sb doped ZnO samples grown with different P(O_2) (1.3 Pa, 0 Pa) to investigate the influence of oxygen on the RT FM. It is found that the sample grown without extra oxygen addition shows enhanced ferromagnetism compared with the sample grown with P(O_2)=1.3 Pa. The FM dependence on oxygen partial pressure can be assigned to the formation of Sb_{Zn}-$2V_{Zn}$. The hypothesis can be verified by the previous work [39], in which the electron concentration decrease with increasing oxygen pressure due to the increase concentration of V_{Zn} related defect like Sb_{Zn}-$2V_{Zn.}$

In conclusion, magnetic behavior of Sb doped ZnO have been studied in theoretically and experimentally. Theoretical calculation revealed that V_{Zn}^{0}, V_{Zn}^{1-} Sb_{O}^{0}, and $(Sb_{Zn}$-$2V_{Zn})^{0}$ could be the cause for the ferromagnetism in Sb doped ZnO material. Experimentally, doping ZnO with 0.5 % Sb doubles the saturation magnetization as compared to the undoped ZnO sample. This is probably due to the enhancement of V_{Zn} concentration by the self-compensation effect as the 0.5 % Sb doped ZnO has degenerate electron concentration ~10^{21} cm^{-3} and V_{Zn} contribute to the ferromagnetism. As the Sb composition increases to 2 %, the saturation magnetization drops. This could be due to the formation of the Sb_{Zn}-$2V_{Zn}$, though it could contribute to ferromagnetism but have a lower magnetic moment as compared to V_{Zn}.

ACKNOWLEDGEMENT

This work was supported by the RGC, HKSAR (GRF 17302115).

References

[1] J.M. Coey, M. Venkatesan, C.B. Fitzgerald, Donor impurity band exchange in dilute ferromagnetic oxides, Nature materials, 4 (2005) 173-179.
[2] J.K. Furdyna, Diluted magnetic semiconductors, Journal of Applied Physics, 64 (1988) R29-R64.
[3] M.M. Yuji Matsumoto, Tomoji Shono, Tetsuya Hasegawa, Tomoteru Fukumura, Masashi Kawasaki, Parhat Ahmet, Toyohiro Chikyow, Shin-ya Koshihara, Hideomi Koinum, Room-TemperatureFerromagnetism in TransparentTransition Metal–DopedTitanium Dioxide, Science, 291 (2001).
[4] H. Ohno, A. Shen, F. Matsukura, A. Oiwa, A. Endo, S. Katsumoto, Y. Iye, (Ga,Mn)As: A new diluted magnetic semiconductor based on GaAs, Applied Physics Letters, 69 (1996) 363-365.
[5] S. Oseroff, R. Calvo, Z. Fisk, F. Acker, Magnetic behavior of Cd1− xMnxSe, Physics Letters A, 80 (1980) 311-313.
[6] R.D. McNorton, J.M. MacLaren, A study of the disordered dilute magnetic semiconductors Zn1− xCrxSe and Zn1− xFexSe, Journal of Physics: Condensed Matter, 21 (2009) 445803.
[7] P. Sharma, A. Gupta, K. Rao, F.J. Owens, R. Sharma, R. Ahuja, J.O. Guillen, B. Johansson, G. Gehring, Ferromagnetism above room temperature in bulk and transparent thin films of Mn-doped ZnO, Nature materials, 2 (2003) 673.
[8] H.-J. Lee, S.-Y. Jeong, C.R. Cho, C.H. Park, Study of diluted magnetic semiconductor: Co-doped ZnO, Applied Physics Letters, 81 (2002) 4020-4022.
[9] Ü. Özgür, Y.I. Alivov, C. Liu, A. Teke, M. Reshchikov, S. Doğan, V. Avrutin, S.-J. Cho, Morkoç, A comprehensive review of ZnO materials and devices, Journal of applied physics, 98 (2005) 11.
[10] K.R. Kittilstved, W.K. Liu, D.R. Gamelin, Electronic structure origins of polarity-dependent high-TC ferromagnetism in oxide-diluted magnetic semiconductors, Nature materials, 5 (2006) 291-297.
[11] A. Di Trolio, R. Larciprete, S. Turchini, N. Zema, Bulk sensitive x-ray absorption and magnetic circular dichroism investigation of Mn- and Co-doped ZnO thin films, Applied Physics Letters, 97 (2010).
[12] K. Ueda, H. Tabata, T. Kawai, Magnetic and electric properties of transition-metal-doped ZnO films, Applied Physics Letters, 79 (2001) 988-990.
[13] S. Ramachandran, A. Tiwari, J. Narayan, Zn0.9Co0.1O-based diluted magnetic semiconducting thin films, Applied Physics Letters, 84 (2004) 5255-5257.
[14] M. Gacic, G. Jakob, C. Herbort, H. Adrian, T. Tietze, S. Brück, E. Goering, Magnetism of Co-doped ZnO thin films, Physical Review B, 75 (2007).
[15] D.A. Schwartz, D.R. Gamelin, Reversible 300 K Ferromagnetic Ordering in a Diluted Magnetic Semiconductor, Advanced Materials, 16 (2004) 2115-2119.
[16] D.C. Kundaliya, S.B. Ogale, S.E. Lofland, S. Dhar, C.J. Metting, S.R. Shinde, Z. Ma, B. Varughese, K.V. Ramanujachary, L. Salamanca-Riba, T. Venkatesan, On the origin of high-temperature ferromagnetism in the low-temperature-processed Mn-Zn-O system, Nature materials, 3 (2004) 709-714.
[17] W. Liu, X. Tang, Z. Tang, Effect of oxygen defects on ferromagnetism of Mn doped ZnO, Journal of Applied Physics, 114 (2013) 123911.
[18] D. Karmakar, S.K. Mandal, R.M. Kadam, P.L. Paulose, A.K. Rajarajan, T.K. Nath, A.K. Das, I. Dasgupta, G.P. Das, Ferromagnetism in Fe-doped ZnO nanocrystals: Experiment and theory, Physical Review B, 75 (2007).

[19] D.B. Buchholz, R.P.H. Chang, J.Y. Song, J.B. Ketterson, Room-temperature ferromagnetism in Cu-doped ZnO thin films, Applied Physics Letters, 87 (2005) 082504.
[20] T.S. Herng, D.C. Qi, T. Berlijn, J.B. Yi, K.S. Yang, Y. Dai, Y.P. Feng, I. Santoso, C. Sanchez-Hanke, X.Y. Gao, A.T. Wee, W. Ku, J. Ding, A. Rusydi, Room-temperature ferromagnetism of Cu-doped ZnO films probed by soft X-ray magnetic circular dichroism, Phys Rev Lett, 105 (2010) 207201.
[21] Y. Tian, Y. Li, M. He, I.A. Putra, H. Peng, B. Yao, S.A. Cheong, T. Wu, Bound magnetic polarons and p-d exchange interaction in ferromagnetic insulating Cu-doped ZnO, Applied Physics Letters, 98 (2011).
[22] J. Yi, C. Lim, G. Xing, H. Fan, L. Van, S. Huang, K. Yang, X. Huang, X. Qin, B. Wang, Ferromagnetism in dilute magnetic semiconductors through defect engineering: Li-doped ZnO, Physical review letters, 104 (2010) 137201.
[23] H. Peng, H. Xiang, S.-H. Wei, S.-S. Li, J.-B. Xia, J. Li, Origin and enhancement of hole-induced ferromagnetism in first-row d 0 semiconductors, Physical review letters, 102 (2009) 017201.
[24] H. Hsu, J.-C.A. Huang, Y. Huang, Y. Liao, M. Lin, C. Lee, J. Lee, S. Chen, L. Lai, C.-P. Liu, Evidence of oxygen vacancy enhanced room-temperature ferromagnetism in Co-doped ZnO, Applied Physics Letters, 88 (2006) 242507.
[25] T. Herng, D.-C. Qi, T. Berlijn, J. Yi, K. Yang, Y. Dai, Y. Feng, I. Santoso, C. Sánchez-Hanke, X. Gao, Room-temperature ferromagnetism of Cu-doped ZnO films probed by soft X-ray magnetic circular dichroism, Physical review letters, 105 (2010) 207201.
[26] X. Yin, Y. Wang, R. Jacobs, Y. Shi, I. Szlufarska, D. Morgan, X. Wang, Massive Vacancy Concentration Yields Strong Room-Temperature Ferromagnetism in Two-Dimensional ZnO, Nano letters, 19 (2019) 7085-7092.
[27] C.-Q. Luo, S.-C. Zhu, C.-H. Lam, F.C.-C. Ling, Ferromagnetic behavior of native point defects and vacancy-clusters in ZnO studied by first principle calculation, Materials Research Express, 7 (2020) 076103.
[28] W. Azeem, C.-Q. Luo, C. Xu, S. Zhou, A. Wagner, M. Butterling, M. Younas, F.C.-C. Ling, Ferromagnetism in undoped ZnO grown by pulsed laser deposition, Materials Research Express, 7 (2020) 056102.
[29] J.H. Park, M.G. Kim, H.M. Jang, S. Ryu, Y.M. Kim, Co-metal clustering as the origin of ferromagnetism in Co-doped ZnO thin films, Applied Physics Letters, 84 (2004) 1338-1340.
[30] M. Younas, L. Zou, M. Nadeem, S. Su, Z. Wang, W. Anwand, A. Wagner, J. Hao, C. Leung, R. Lortz, Impedance analysis of secondary phases in a Co-implanted ZnO single crystal, Physical Chemistry Chemical Physics, 16 (2014) 16030-16038.
[31] B.B. Straumal, A. Myatiev, P. Straumal, A. Mazilkin, S. Protasova, E. Goering, B. Baretzky, Grain boundary layers in nanocrystalline ferromagnetic zinc oxide, JETP letters, 92 (2010) 396-400.
[32] B. Straumal, S. Protasova, A. Mazilkin, A. Myatiev, P. Straumal, G. Schütz, E. Goering, B. Baretzky, Ferromagnetic properties of the Mn-doped nanograined ZnO films, Journal of Applied Physics, 108 (2010) 073923.
[33] M. Younas, J. Shen, M. He, R. Lortz, F. Azad, M. Akhtar, A. Maqsood, F. Ling, Role of multivalent Cu, oxygen vacancies and CuO nanophase in the ferromagnetic properties of ZnO: Cu thin films, RSC Advances, 5 (2015) 55648-55657.
[34] N. Sánchez González, Estados electrónicos y magnéticos en superficies de óxidos: ZnO, (2016).
[35] H. Pan, J. Yi, L. Shen, R. Wu, J. Yang, J. Lin, Y. Feng, J. Ding, L. Van, J. Yin, Room-temperature ferromagnetism in carbon-doped ZnO, Physical review letters, 99 (2007) 127201.
[36] J.B. Yi, C.C. Lim, G.Z. Xing, H.M. Fan, L.H. Van, S.L. Huang, K.S. Yang, X.L. Huang, X.B. Qin, B.Y. Wang, T. Wu, L. Wang, H.T. Zhang, X.Y. Gao, T. Liu, A.T. Wee, Y.P. Feng, J. Ding, Ferromagnetism in dilute magnetic semiconductors through defect engineering: Li-doped ZnO, Phys Rev Lett, 104 (2010) 137201.
[37] F.X. Xiu, Z. Yang, L.J. Mandalapu, D.T. Zhao, J.L. Liu, W.P. Beyermann, High-mobility Sb-doped p-type ZnO by molecular-beam epitaxy, Applied Physics Letters, 87 (2005).

[38] X. Pan, Z. Ye, J. Li, X. Gu, Y. Zeng, H. He, L. Zhu, Y. Che, Fabrication of Sb-doped p-type ZnO thin films by pulsed laser deposition, Applied Surface Science, 253 (2007) 5067-5069.
[39] C. Luo, L.-P. Ho, F. Azad, W. Anwand, M. Butterling, A. Wagner, A. Kuznetsov, H. Zhu, S. Su, F.C.-C. Ling, Sb-related defects in Sb-doped ZnO thin film grown by pulsed laser deposition, Journal of Applied Physics, 123 (2018) 161525.
[40] H. Liu, N. Izyumskaya, V. Avrutin, Ü. Özgür, A. Yankovich, A. Kvit, P. Voyles, H. Morkoç, Donor behavior of Sb in ZnO, Journal of Applied Physics, 112 (2012) 033706.
[41] S. Limpijumnong, S.B. Zhang, S.H. Wei, C.H. Park, Doping by large-size-mismatched impurities: the microscopic origin of arsenic- or antimony-doped p-type zinc oxide, Phys Rev Lett, 92 (2004) 155504.
[42] S. Limpijumnong, S. Zhang, S.-H. Wei, C. Park, Doping by large-size-mismatched impurities: the microscopic origin of arsenic-or antimony-doped p-type zinc oxide, Physical review letters, 92 (2004) 155504.
[43] A.B. Yankovich, B. Puchala, F. Wang, J.-H. Seo, D. Morgan, X. Wang, Z. Ma, A.V. Kvit, P.M. Voyles, Stable p-type conduction from Sb-decorated head-to-head basal plane inversion domain boundaries in ZnO nanowires, Nano letters, 12 (2012) 1311-1316.
[44] R. Jacobs, B. Zheng, B. Puchala, P.M. Voyles, A.B. Yankovich, D. Morgan, Counterintuitive reconstruction of the polar O-terminated ZnO surface with zinc vacancies and hydrogen, The journal of physical chemistry letters, 7 (2016) 4483-4487.
[45] R.R. Reeber, Lattice parameters of ZnO from 4.2 to 296 K, Journal of applied physics, 41 (1970) 5063-5066.
[46] A. Kohan, G. Ceder, D. Morgan, C.G. Van de Walle, First-principles study of native point defects in ZnO, Physical Review B, 61 (2000) 15019.
[47] C.G. Van de Walle, J. Neugebauer, First-principles calculations for defects and impurities: Applications to III-nitrides, Journal of applied physics, 95 (2004) 3851-3879.
[48] K. Matsunaga, T. Tanaka, T. Yamamoto, Y. Ikuhara, First-principles calculations of intrinsic defects in Al 2 O 3, Physical Review B, 68 (2003) 085110.
[49] Y. Kumagai, F. Oba, Electrostatics-based finite-size corrections for first-principles point defect calculations, Physical Review B, 89 (2014) 195205.
[50] C. Freysoldt, J. Neugebauer, C.G. Van de Walle, Fully ab initio finite-size corrections for charged-defect supercell calculations, Physical review letters, 102 (2009) 016402.
[51] I.G. Batyrev, A. Alavi, M.W. Finnis, Equilibrium and adhesion of Nb/sapphire: The effect of oxygen partial pressure, Physical Review B, 62 (2000) 4698.
[52] M. Finnis, A. Lozovoi, A. Alavi, The oxidation of NiAl: What can we learn from ab initio calculations?, Annu. Rev. Mater. Res., 35 (2005) 167-207.
[53] K. Johnston, M.R. Castell, A.T. Paxton, M.W. Finnis, Sr Ti O 3 (001)(2× 1) reconstructions: First-principles calculations of surface energy and atomic structure compared with scanning tunneling microscopy images, Physical Review B, 70 (2004) 085415.
[54] D. Kim, J.-h. Yang, J. Hong, Ferromagnetism induced by Zn vacancy defect and lattice distortion in ZnO, Journal of Applied Physics, 106 (2009) 013908.
[55] R. Deng, X. Han, J. Qin, B. Yao, Z. Ding, Y. Li, Cation impurity-defect complex induced ferromagnetism and hopping conduction in Sb-doped ZnO synthesized under high pressure, Journal of Alloys and Compounds, 823 (2020) 153713.
[56] P. Nakarungsee, G. Chen, T. Herng, J. Ding, I. Tang, S. Talabthong, S. Thongmee, Sb substitution into ZnO nano-composite: Ferromagnetic behavior, Journal of Magnetism and Magnetic Materials, 397 (2016) 79-85.
[57] G.-H. Ji, Z.-B. Gu, M.-H. Lu, D. Wu, S.-T. Zhang, Y.-Y. Zhu, S.-N. Zhu, Y.-F. Chen, Ferromagnetism in Mn and Sb co-doped ZnO films, Journal of Physics: Condensed Matter, 20 (2008) 425207.
[58] D.C. Look, K. Leedy, L. Vines, B. Svensson, A. Zubiaga, F. Tuomisto, D.R. Doutt, L. Brillson, Self-compensation in semiconductors: The Zn vacancy in Ga-doped ZnO, Physical Review B, 84 (2011) 115202.

[59] C. Pak, S. Su, C. Ling, Y. Lu, D. Zhu, Post-growth annealing study of heavily Ga-doped zinc oxide grown by radio frequency magnetron sputtering, Journal of Physics D: Applied Physics, 46 (2013) 135104.